Meteorol Atmos Phys (2013) 122:159–173
DOI 10.1007/s00703-013-0282-4

ORIGINAL PAPER

Role of the cloud adjustment time scale in simulation of the interannual variability of Indian summer monsoon

Deepesh Kumar Jain · Arindam Chakraborty · Ravi S. Nanjundiah

Received: 26 October 2012 / Accepted: 3 September 2013 / Published online: 1 October 2013

Abstract The simulation of precipitation in a general circulation model relying on relaxed mass flux cumulus parameterization scheme is sensitive to cloud adjustment time scale (CATS). In this study, the frequency of the dominant intra-seasonal mode and interannual variability of Indian summer monsoon rainfall (ISMR) simulated by an atmospheric general circulation model is shown to be sensitive to the CATS. It has been shown that a longer CATS of about 5 h simulates the spatial distribution of the ISMR better. El Niño Southern Oscillation–ISMR relationship is also sensitive to CATS. The equatorial Indian Ocean rainfall and ISMR coupling is sensitive to CATS. Our study suggests that a careful choice of CATS is necessary for adequate simulation of spatial pattern as well as interannual variation of Indian summer monsoon precipitation.

1 Introduction

The Indian economy relies heavily on its agricultural production which depends on the Indian summer monsoon rainfall (ISMR) for natural irrigation (Gadgil 2003). The importance of predicting the phenomenon can not be over emphasized. For example, it has been seen that variation of intensity of rainfall at intraseasonal time scale can produce droughts and floods over Indian region (e.g., Bhanu Kumar et al. 2010). However, state-of-the-art general circulation models (GCM) have difficulty in forecasting daily intensity of Indian summer monsoon and its diurnal variability more than 3 days in advance (Chakraborty 2010). In a numerical GCM, the prediction of precipitation on a daily to interannual to decadal time scales depends on the way the interaction between various components of the climate system have been parameterized (Tebaldi and Knutti 2007). The interannual to decadal variability of ISMR is sensitive to boundary conditions such as sea surface temperature (SST), snow cover over Eurasian region, and soil moisture (Hahn and Shukla 1976; Shukla and Mintz 1982; Rasmusson and Carpenter 1983). In many recent studies, the basic feature of ISMR is well simulated (Kang et al. 2002). The magnitude and variability of simulated ISMR in GCM's, however, is still not satisfactory.

The Indian region is one of the most convectively active regions of the tropics and simulation of precipitation on any time scale by a GCM depends not only on the choice of the cumulus parameterization scheme, but also on the various associated parameters in the scheme (Ratnam et al. 2009; Das et al. 2001). Using Relaxed Arakawa–Schubert (RAS) parameterization (Moorthi and Suarez 1992), Pattanaik and Satyan (2004) studied the sensitivity of the model simulated precipitation on the choice of critical cloud work function values in Center for Ocean–Land-Atmosphere GCM and found that the excessive rainfall over Bay of Bengal (BoB) can be decreased by modifying the values of critical cloud work function and re-evaporation ratio. Many previous studies (Jain et al. 2012; Mishra and Srinivasan 2010; Lee et al. 2008) have suggested that the choice of convective adjustment time scale (τ_{adj}) has significant impact on precipitation. Mishra and Srinivasan (2010) used Zhang and McFarlane (1995) convection scheme in Community Atmospheric Model version 3 in an

Responsible editor: S. Hong.

D. K. Jain · A. Chakraborty (✉) · R. S. Nanjundiah
Centre for Atmospheric and Oceanic Sciences and Divecha Centre for Climate Change, Indian Institute of Science, Bangalore, India
e-mail: arch@caos.iisc.ernet.in

aqua-planet configuration and suggested that a value of 8 h instead of 1–2 h for τ_{adj} produced better simulations. In their findings, increasing the value of τ_{adj} increased the shallow and large scale precipitation due to accumulation of moisture content in the atmosphere.

Moorthi and Suarez (1992) studied the effect of τ_{adj} in RAS by changing the relaxation parameter. Relaxation parameter is the fraction of model time step to τ_{adj}. They used a 9-layer model to show the evolution of precipitation rate, entrainment parameter, precipitation rate, and cloud work function. The evolution of these variables within model time step was sensitive to the choice of τ_{adj}. A relaxation parameter was used to represent the effect of τ_{adj}. A smaller relaxation parameter (larger τ_{adj}) allowed for lesser adjustment per cloud type. This resulted into more number of cloud types (iterations) being called in one time step. In a recent study by Jain et al. (2012), the precipitation rate was found highly sensitive to the choice of relaxation parameter. The choice of a smaller relaxation parameter allowed the neglect of rate of change of entrainment parameter in the kernel calculations (Moorthi and Suarez 1992) and simplified it. Studies by Moorthi and Suarez (1992) and Jain et al. (2012) emphasized the need for a cloud type dependent τ_{adj}.

In our previous study in Jain et al. (2012), we experimented extensively on the effect of τ_{adj} on the simulation of June–September (ISMR period) of 2008 precipitation over the tropics using the National Center for Environmental Prediction (NCEP) seasonal forecast model (SFM). It was found that the precipitation over Indian region, BoB and West Pacific was highly sensitive to τ_{adj}. A longer τ_{adj} allowed for precipitation over BoB closer to observed one. It was suggested that a longer τ_{adj} gave better result over India. They suggested a linear τ_{adj} based on the linear dependence between τ_{adj} and the cloud height. The RAS scheme was made to select τ_{adj} based on the cloud height in the proposed linear τ_{adj} simulations.

In the present study, we examine the sensitivity of simulated annual and interannual variability of ISMR over India by a GCM to the choice of relaxation parameter (τ_{adj}). The model used for the present study is described in the next section. The role of relaxation parameter in controlling the grid scale precipitation in RAS is described in Sect. 3. Experimental details are provided in Sect. 4. Section 5 discusses observational datasets used in this study for validating the results. Results of this study are discussed in Sect. 6 followed by the major conclusions.

2 Model description

The SFM from NCEP used for the present study was run at T62L28 resolution. The model has 28 unequal vertical sigma levels and a horizontal resolution of 1.875°. For uniform resolution throughout the globe, the model uses a reduced grid. Chou (1992) short-wave radiation parameterization is used in the experiment while the long-wave parameterization is from Chou and Suarez (1994). Planetary boundary layer as parameterized by Hong and Pan (1996) is used. Cloud fraction is based on Slingo (1987). Mountain induced gravity wave drag parameterization is by Alpert et al. (1988). Land process parameterization by Pan and Mahrt (1987) is used in the model. Smoothed mean orography is used in the study and ozone is prescribed using climatology. The RAS cumulus parameterization scheme is based on Moorthi and Suarez (1992). Semi-implicit time integration is used for model dynamics. Kanamitsu et al. (2002) provides detailed description of the model.

3 Role of τ_{adj} in RAS Parameterization scheme

The role of τ_{adj} was discussed in detail in Jain et al. (2012). We give a brief description here for completeness. The RAS cumulus parameterization scheme is based on the theory of Moorthi and Suarez (1992). In the original Arakawa and Schubert (1974) (AS) scheme, cloud type in the spectrum were distinguished according to fractional entrainment rate. This caused the height of the cloud to be a dependent parameter. Instead, in RAS, a cloud type is distinguished using the height at which it detrains and fractional entrainment rate becomes the dependent parameter. All the liquid water is assumed to be carried to the top of the cloud from where a fraction is allowed to precipitate and remaining water is evaporated into the environment.

Moorthi and Suarez (1992) simplified AS in such a way that rather than reaching a final quasi-equilibrium state in the AS sense, the environment is relaxed towards that state every time the scheme is invoked. Multiple cloud types selected randomly and iteratively in a single time step, one after the other, relaxes the environment to a quasi-equilibrium state. The relaxation time depends on the model time step, the prescribed adjustment time scale and the frequency at which each cloud type is invoked. The relaxation parameter can be represented as Moorthi and Suarez (1992)

$$\alpha = \triangle t/\tau_{adj} \quad (1)$$

where $\triangle t$ is the model time step or the iteration time step and τ_{adj} represents the prescribed cloud adjustment time scale (CATS 10^3–10^4 s). It is emphasized that τ_{adj} can be cloud type dependent.

A cloud type is distinguished by the level at which it detrains. An *i*th cloud type detrains at *i*th level in an *N* layer

model. The rate of change of prognostic variables, potential temperature (θ) and specific humidity (q), is calculated as

$$\left(\frac{\partial\theta}{\partial t}\right)_c = \alpha\frac{m_B(\lambda_i)\triangle\lambda_i}{c_p P}\Gamma_s(P), \tag{2}$$

and

$$\left(\frac{\partial q}{\partial t}\right)_c = \alpha\frac{1}{L}m_B(\lambda_i)\triangle\lambda_i[\Gamma_h(P) - \Gamma_s(P)], \tag{3}$$

The liquid water mixing ratio, $l(P_D)$, at the top of the detrainment level (pressure level P_D) is calculated as

$$\begin{aligned} l(P_D) &= l^c_\lambda(P_D) \\ &= \frac{1}{\eta_\lambda(P_D)}\left[q(P_B) + \frac{c_p}{g}\lambda\int_{P_D}^{P_B}\theta q(P)\mathrm{d}P\right] - q^*(P_D) \end{aligned} \tag{4}$$

where λ is the fractional entrainment rate, $\eta_\lambda(P_D)$ represents the normalized mass flux of the cloud normalized by the value at the cloud base, $q(P_B)$ represents specific humidity at the cloud base and $q^*(P_D)$ is the saturation specific humidity. $\Gamma_h(P)$ and $\Gamma_s(P)$ represents the tendencies of the environmental moist static energy (h) and dry static energy (s) per unit cloud base mass flux [Eqs. 27 and 28 in Moorthi and Suarez (1992)].

The precipitation, R_i, is parameterized as

$$R_i = M_B(i)r_i l_{i,i} \tag{5}$$

where M_B is the cloud base mass flux. r_i is cloud type dependent parameter assumed as

$$r_i = \begin{cases} 1.0 & \text{if } p_i < 500 \\ 0.80 + (800 - p_i)/1,500 & \text{if } 500 < p_i < 800 \\ 0.80 & \text{if } p_i > 800 \end{cases} \tag{6}$$

where p(hPa) is pressure. Equations 2–4 show that the choice of α affects the rate of change of q and θ. Hence, the rate of change of liquid water mixing ratio $l(P_D)$ depends on α. It can be seen that the relation between $l(P_D)$ and α is non-linear.

4 Experimental details

The experiment was started by giving an Atmospheric Model Intercomparison Project (AMIP) style run starting on 1st January, 1982. The model was integrated for 28 years till 31st December, 2009. Monthly mean SST to force the model at ocean surface was obtained from Reynolds and Smith (1994) and was interpolated linearly to the model time step. Initial conditions were taken from NCEP reanalysis. Diagnostic variables are output as daily averages (once every day). A 30 min model time step was used for the integrations and the output was saved once a day. The focus of the present paper is to study the sensitivity of annual and interannual variability of the simulated precipitation over India during the Boreal summer monsoon season to the choice of relaxation parameter. We have done sensitivity studies between two simulations, one with $\alpha = 0.10$ and the other with $\alpha = 0.30$. The two simulations will be referred to as the AL1 and the AL3. We call the case in which $\alpha = 0.30$ as the control case or the default value of α. $\alpha = 0.10$ refers to τ_{adj} of 300 min while in the control case τ_{adj} is 100 min.

5 Data sets

Rain gauge based gridded precipitation obtained from IMD was used to compare with model output. Since the IMD's data is available only over land, the global dataset from Global Precipitation Climatology Project (GPCP), a merged product of rain gauge and satellite estimates, is used for validating results over ocean. The horizontal resolution of satellite–gauge combined estimates from GPCP is 2.5° × 2.5°. Combined precipitation data GPCP version 2.1 is available as long term monthly mean. It has a temporal extent from January 1979 to September 2009. Since the model resolution is different than that of GPCP's and that of IMD's, these datasets are regridded to model resolution for comparisons. We have IMD spatial data from 1982 to 2004. Hence, for the first four figures where we have shown the climatology, mean seasonal cycle, mean daily cycle, and mean power spectrum, we have analyzed data during this duration. Since these values are mean over 23 years, we believe they will not be significantly different from 28 years mean values. For Fig. 5, we needed ISMR mean values for 2005 onwards and we took the seasonal mean values from IMD's website (http://www.imd.gov.in/section/nhac/dynamic/Monsooni_frame.htm). Where ever we required spatial observations for 2005 onwards, we have taken GPCP.

6 Results

6.1 Climatological mean precipitation

Climatological mean precipitation during June–September over India can be seen in Fig. 1. The spatial correlation between IMD data and GPCP data is 0.76. We consider the interannual variation of mean rainfall during June–September. The observed and simulated (AL3 and AL1) mean climatological precipitation over South Asian region is shown in Fig. 1. The orographic rainfall over Western Ghats and Himalayan foothills is distinctively clear in both IMD and GPCP observations. GPCP also shows the high

precipitation regions over the ocean such as BoB, equatorial Indian Ocean (EIO), and Arabian Sea. In the control case (AL3), the model is able to simulate these features. However, the rainfall is highly overestimated over BoB and Arabian Sea. The EIO rainfall seems consistent with the observations, though the rainfall band as a whole seems to have shifted west when compared to observations. As can be seen in Fig. 2, the root mean square error (RMSE) between control simulation and GPCP for the region shown in the figure is 5.9 mm/day. The spatial correlation (SC) over the same region is 0.63. When the value of τ_{adj} is increased to 300 min (α reduced to 0.10), the excess rainfall over the head bay disappears. The magnitude of rainfall over BoB, Western Ghats, and EIO is reasonably close to GPCP with AL1 simulation. The RMSE is reduced substantially to 3.5 mm/day, and SC has increased to 0.65. A recent study by Jain et al. (2012) shows that lower value of cloud relaxation parameter (in AL1) in this model performs better than $\alpha = 0.30$ in simulating precipitation over entire tropics.

6.2 Annual precipitation over India

The January–December monthly mean precipitation from IMD observations and model simulations averaged from 1982 to 2004 is shown in Fig. 2. More than 80 % of the annual precipition occurs between June and September. In IMD observations, the peak precipitation of the ISM season (June–September) is seen in July. Both the simulations (AL1 and AL3) seems to overestimate precipitation throughout the season. In AL3, the peak precipitation lags by a month and occurs in August. The peak precipitation in AL1 simulation occurs in July in agreement with IMD observations. This results in temporal correlation between AL1 and IMD observations for the ISM season to be 0.97, much better compared to that between AL3 and observations, where it is 0.78. Getting the phase of the peak precipitation correct is one of the very significant improvements AL1 provides over AL3. Overall, the two simulations over-estimate rainfall throughout the year. Figure 3 shows climatology of daily

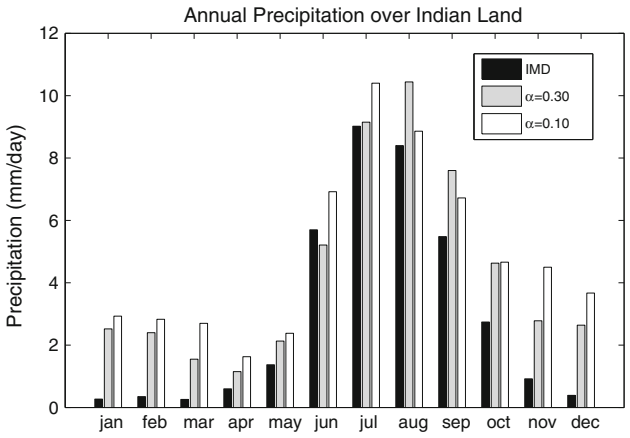

Fig. 2 Mean monthly precipitation over the Indian region (grid points where the IMD precipitation is defined within the domain 70–90E, 8–28N, as can be seen in the left most panel of Fig. 1) averaged over the years from 1982 to 2004

JJAS precipitation over India (70–90E and 8–28N, land part). It can be seen that the precipitation peaks in the month of July in IMD data. AL1 also simulates the peak precipitation in July, while the control simulation (AL3) simulates peak precipitation in August. However, it can be seen that the magnitude of daily precipitation in AL3 is nearer to IMD observations for June and July, whereas for the next 2 months, AL1 simulated precipitation is nearer to the observations. The daily time correlation between simulated precipitation in AL1 shows significant improvement over AL3 with a value of 0.87 for AL1 compared to 0.67 for AL3. So, it can be said that AL1 improves both seasonal and daily precipitation simulations compared to AL3.

6.3 Effect of CATS on ISMR

In Jain et al. (2012), we had seen that rainfall over oceans increased while that over land decreased when we employed faster CATS. The major difference was seen in the rainfall over BoB and Indian land. The reason for this behavior can be attributed to the fact that when we use faster CATS, the

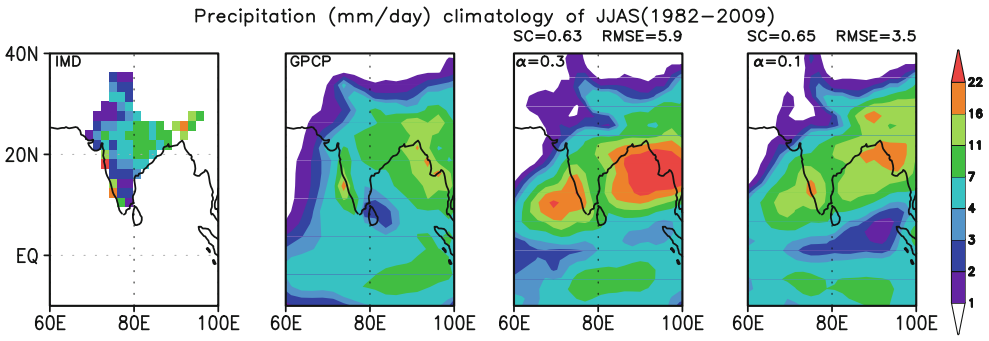

Fig. 1 Climatology mean of rain rate (mm/day) from IMD (1982–2004), GPCP, and the two model simulations with $\alpha = 0.10$ and 0.30 over Indian region for the period of June–September, averaged from 1982 to 2009. For calculation of SC and RMSE (in mm/day), data from GPCP and IMD were regridded to model resolution

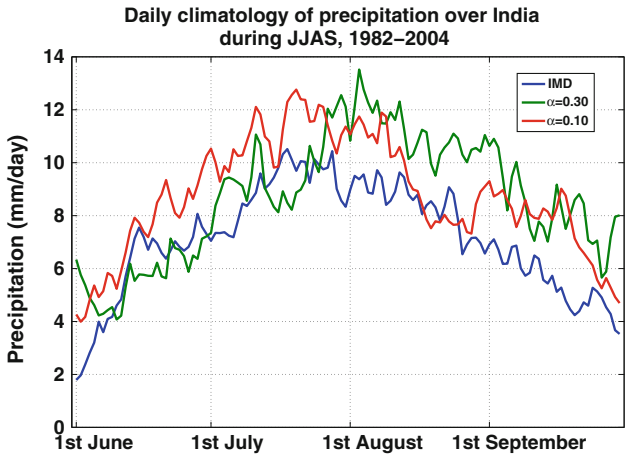

Fig. 3 Daily precipitation over the Indian region (grid points where the IMD precipitation is defined within the domain 70–90E, 8–28N, as can be seen in the left most panel of Fig. 1) in June–September averaged over the years 1982–2004

convective available potential energy is consumed faster and the moisture is precipitated faster. Now, the source of moisture for Indian land is from oceans (BoB and Indian Ocean). If we use a faster CATS, most of the moisture precipitates over ocean. Less moisture is available to precipitate over land. Cloud fraction can be representative of the dominant cloud type present over a region. Figure 4 shows difference between $\alpha = 0.10$ and $\alpha = 0.50$ low, medium, and high cloud cover from control ($\alpha = 0.30$) for JJAS, 2008. The results shown in the figure are five ensemble mean starting from 27 March to 31 March, 2008. The cloud cover is calculated using Slingo (1987) after precipitation has been calculated in the model using RAS. It can be seen that over ocean, cloud cover at all the levels increase as we increase the cloud relaxation parameter α (or reduce CATS). This behavior is expected since a faster CATS allows for faster conversion of available moisture into precipitation in the model. This results in more clouds and precipitation over oceans. Also refer to Fig. 7 of Jain et al. (2012) for similar result. We believe this to be the effect of CATS on ISMR. In the Fig. 5, we also show the frequency distribution of low and high cloud cover in percentage from $\alpha = 0.10$ and $\alpha = 0.30$ simulations, and observed data from International Satellite Cloud Climatology Project (ISCCP). It can be easily seen that a higher relaxation parameter (0.30) produces more of high and low cloud fraction over BoB. The cloud fraction most favored by $\alpha = 0.10$ is 0–10 %, which is very similar to the one observed in ISCCP, whereas it is 50–60 % in control. The difference is not very distinct over land.

6.4 Intraseasonal variability of ISMR

Many studies have been performed to study and emphasize the relationship between intraseasonal and interannual variability of Asian summer monsoon (Goswami and Ajaya Mohan 2001; Yoo et al. 2010). Mishra (2011) showed the sensitivity of interannual variability of ISMR to model time step. Whether choosing different CATS in the simulation can affect the intraseasonal mode is a worthwhile question. In Fig. 6, the mean of power spectra of the 23 years (1982–2004) daily precipitation over India during June-September from IMD data, and model output with AL1 and AL3 is shown. For the analysis of intraseasonal variability in the model, the data is filtered for 10–90 days variability. All the lower frequencies above 90 days and higher frequencies below 10 days period are filtered out using the fast-Fourier transform (FFT) method. Then the inverse FFT was performed to regenerate the data. To specifically analyze the filtered data for Indian summer monsoon, we took 184 days from 1st May to 31st Oct of 23 years. The spectrum shown in the Fig. 6 is the mean of 23 spectrum corresponding to those 23 years. Also shown in this figure is the red noise spectrum (the upper 95 % confidence band of a Markov spectrum). In the IMD data, it is observed that the peak occurs at 23 days time period. IMD data also shows a local maxima in power near 37 days time period. To see what happens when we increase the time of cloud adjustment in the model, the spectra for $\tau_{adj} = 100$ and 300 min (AL3 and AL1) are also shown. It can be seen that the peak occurs at 20 days time period when we use faster adjustment rate in AL3 and it occurs at 25 days when we decrease the adjustment rate in AL1. This shows that in the model, modifying the adjustment time scale (which is few hours) can actually modify the intraseasonal mode of variability. In our simulations, the only difference between the two simulations is the value of α. Hence, we think that changing α can modify the intra-seasonal variability mode in the model and slower rate of adjustment favors slower mode of variability.

We find that change in α changes interannual variability (Fig. 7). Previous studies have shown that interannual variability is related to changes in intraseasonal variation (Goswami and Ajaya Mohan 2001; Yoo et al. 2010). In our simulations, modification of α changes the intraseasonal pattern and this leads to changes in simulated interannual variability. Hence, increasing the rate at which a given cloud work function (normalized convective available potential energy) is consumed can modify the intraseasonl variability mode in the model. A slower rate of adjustment favors slower mode of variability.

6.5 Interannual variability of ISMR and its relationship with ENSO

The relationship between the ENSO and ISMR has always been of interest to Monsoon researchers. Many studies have found that a strong El-Niño event is usually

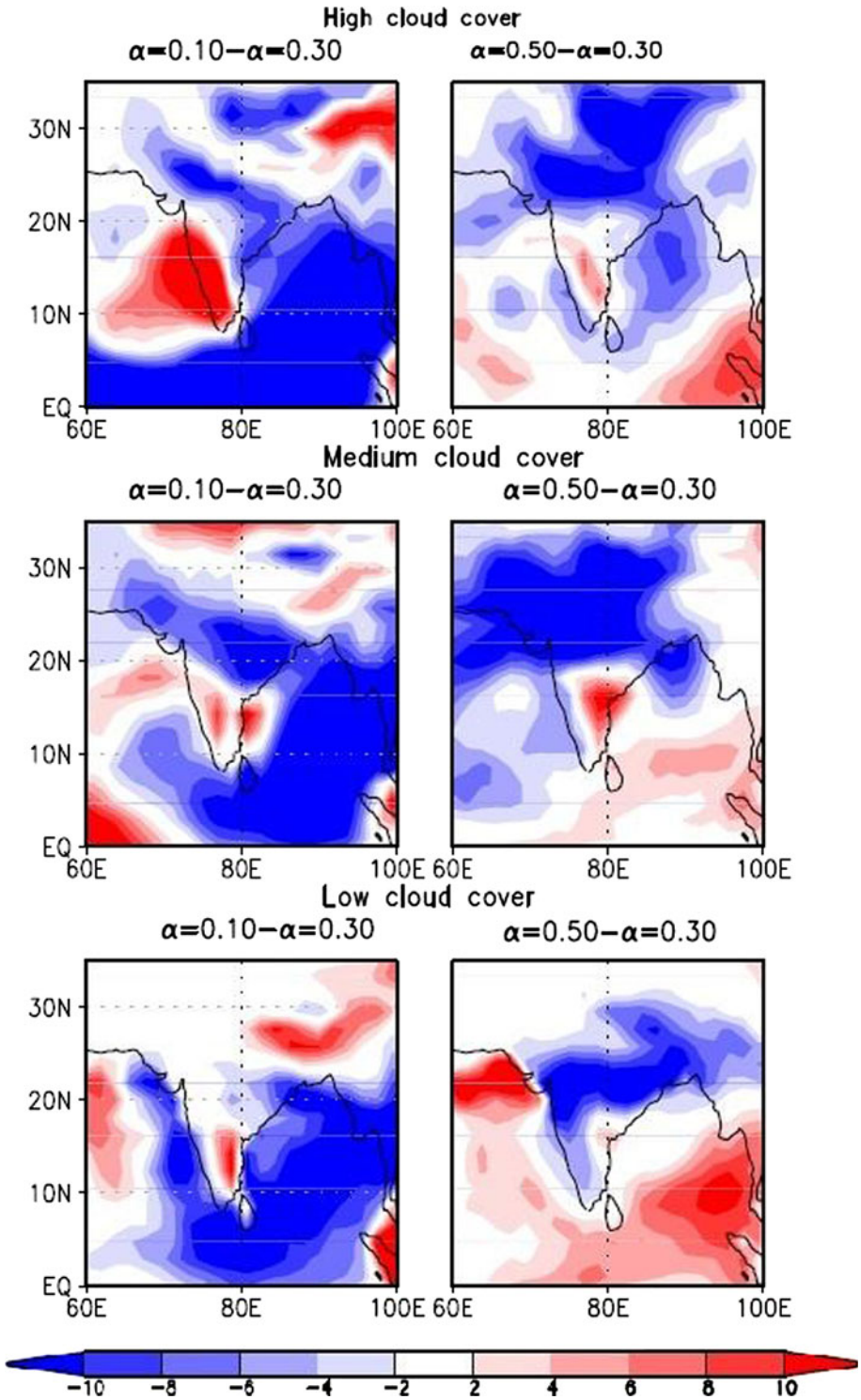

Fig. 4 Difference between $\alpha = 0.10$ and $\alpha = 0.50$ simulated low, medium, and and high cloud cover from the control ($\alpha = 0.30$) for JJAS, 2008

associated with deficit in rainfall over India (Ding 2007; Gadgil et al. 2007; Ihara et al. 2007, 2008; Suppiah 1996; Zubair 2002). In Fig. 7, we show the interannual variability of normalized rainfall anomaly over Indian land (from 70–90E and 8–28N). The anomalies are calculated as the difference between mean June-September precipitation for that particular year from climatological mean of 28 years (1982–2009). The figure also shows the interannual variability of Niño 3.4 region SST anomaly. Niño 3.4 SST anomaly is referred to as ENSO index in this paper. ENSO index is the negative of the SST anomaly of the Nino 3.4 region bounded by 120W–170W and 5S–5N. The major El-Nino and La-Nina events in this 28 years period are marked in the Fig. 7. It can be easily seen that in all the

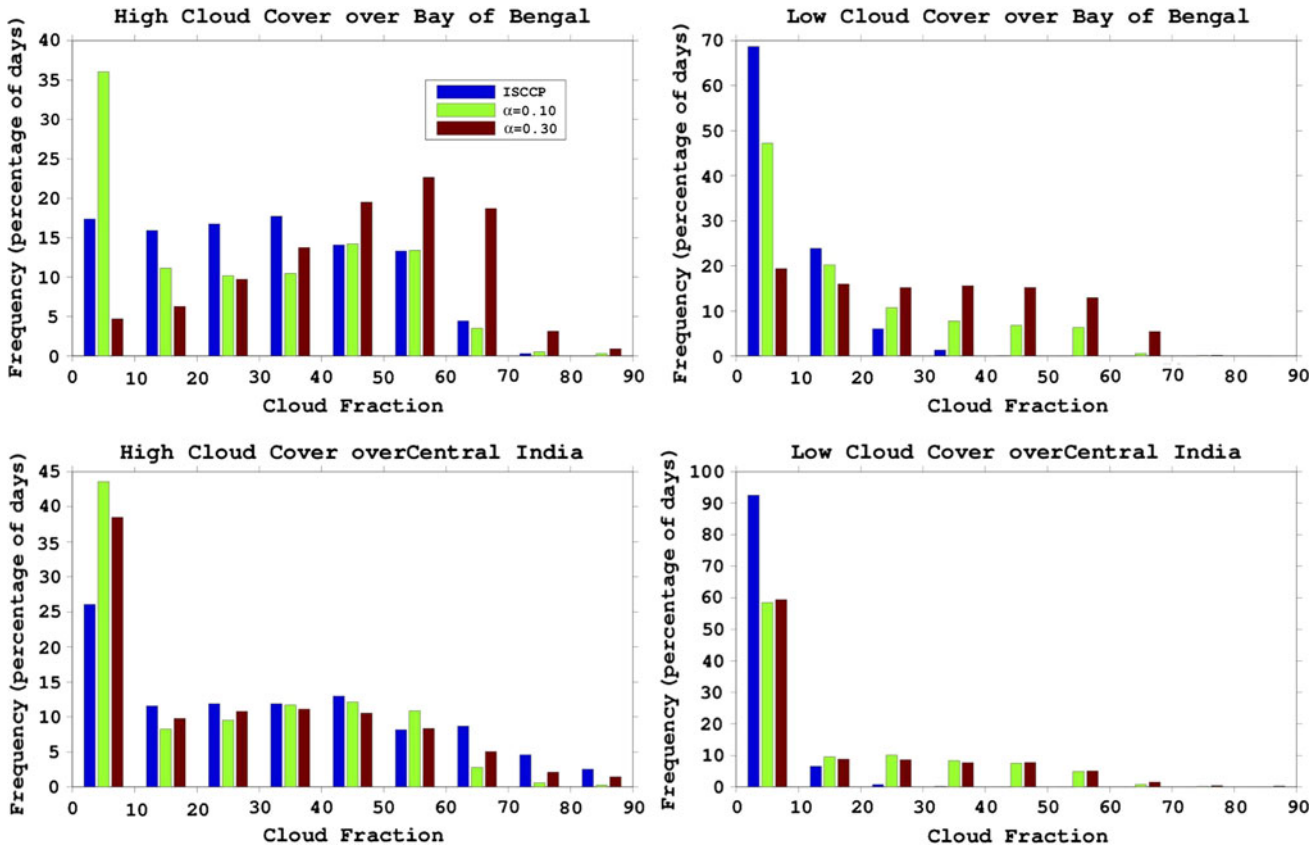

Fig. 5 The frequency distribution of the high and low cloud cover over central BoB (8–18N, 85–95E) and Central India (18–24N, 75–85E) for 2008. The change in cloud cover over BoB is substantial for two relaxation parameters

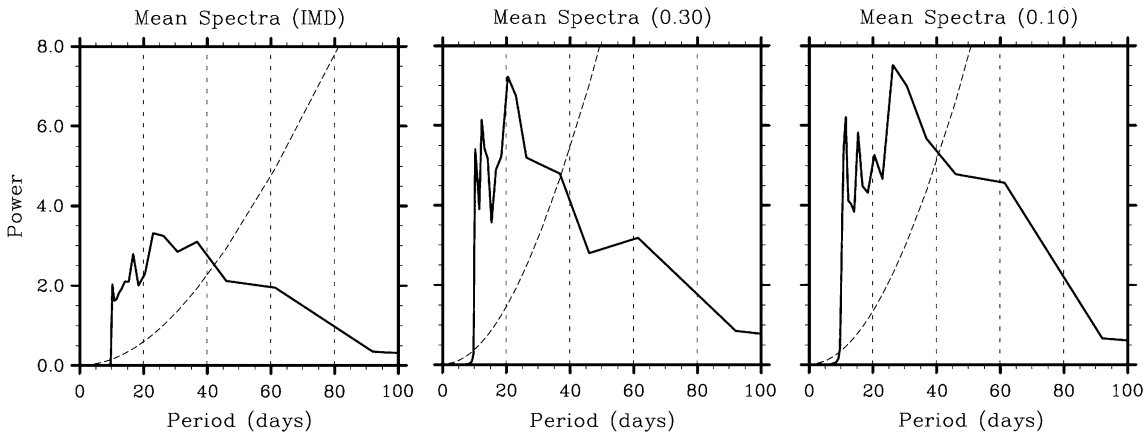

Fig. 6 Power spectrum of filtered (10–90 days) precipitation from daily model output and IMD data over the Indian region (70–90E and 8–28N, land part) from 1982 to 2004. *Dashed line* shows the upper 95 % confidence band on a Markov spectra

major El-Nino years, except 1994 (weak event) and 1997 (strong event), the rainfall over India was below normal. It was shown in Gadgil et al. (2007) that the excess rainfall in those two events was the result of strong EIO Oscillation (EQUINOO) (Gadgil et al. 2007). A strong La-Nina event should conversely be associated with excess rainfall as can be seen in the figure. It can be seen that the La-Nina event of 1988 has excess rainfall. However, in the La-Nina events of 1998–1999, the monsoon was near normal.

In the simulations, both the cases (AL1 and AL3) are able to capture the sign of 1982 and 1983 rainfall anomaly. The deficit of 1982 can be associated with a strong El-Niño

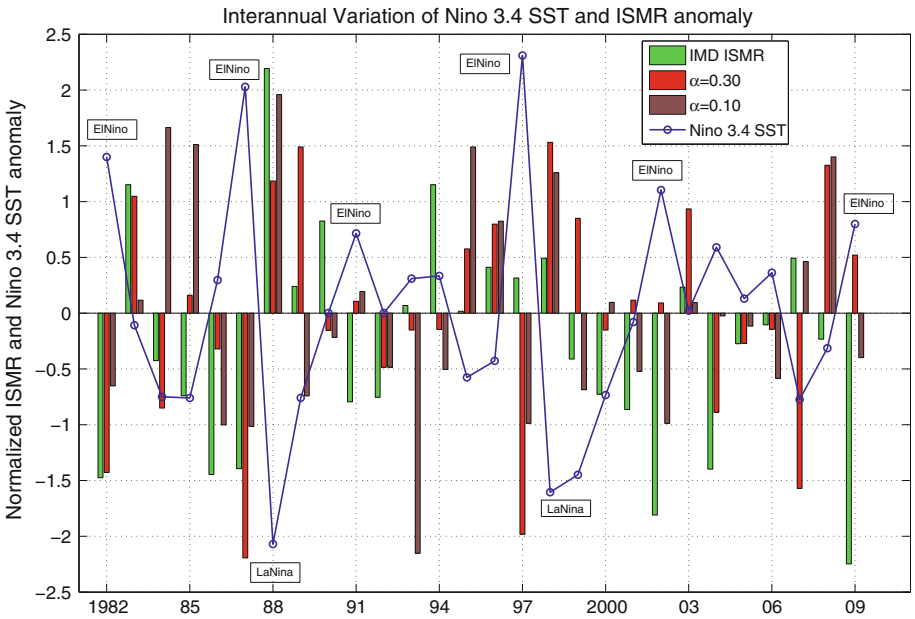

Fig. 7 Interannual variation of June–September mean precipitation (normalized by standard deviation) over Indian landmass (1982–2009) and Niño 3.4 SST anomaly. El-Nino and La-Nina years are marked

event. For these 2 years, the magnitude of deficit captured by AL3 simulation is closer to IMD observations as compared to that of AL1 simulation. AL1 simulation underestimates the deficit for 1982 and excess for 1983 by at least 1 SD. The deficit of 1984 is also captured by AL3 simulation, while AL1 simulation gets it completely wrong. In the El-Nino event of 1987, AL3 simulation shows much larger deficit compared to observations. The magnitude and sign are closer to the observed values in AL1 simulations. In the following two consecutive El-Niño events i.e. 1991 and 1994 (weak event not marked in the figure), both the simulations get the sign of the anomaly wrong. In one of the strongest El-Nino event 1997, the observed rainfall is near normal. While both the simulations get the sign of anomaly wrong, AL3 simulation shows much larger deficit compared to that shown by AL1 simulation. AL1 simulation captured the 2002 rainfall deficit well. In 2009, AL1 simulation gets the sign of the anomaly right while in AL3 simulations the sign is opposite to that of IMD observations. In AL3, the time correlation between Nino 3.4 SST anomaly and rainfall anomaly is -0.66 and it is -0.62 in AL1. Based on this correlation, we can say that model simulation of ISMR is more sensitive to El-Nino, when α is set to 0.30. The choice of α does not seem to have much effect on the simulations during La-Nina years.

6.6 Distribution of excess and drought years in simulations

We consider ISMR events having deviation (normalized with standard deviation) <-1 from climatology mean JJAS precipitation over India as drought years and similarly those

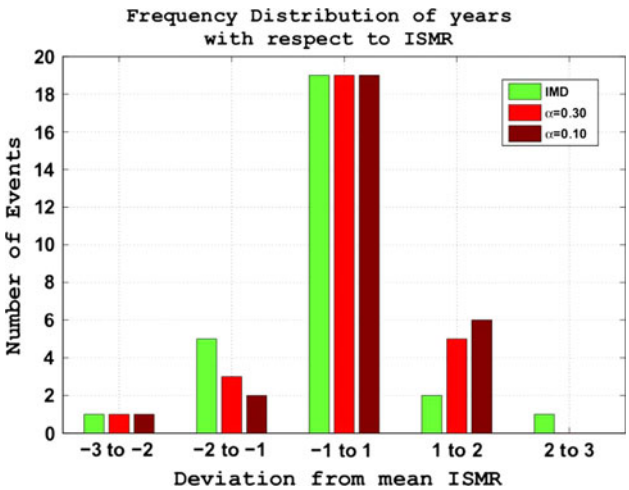

Fig. 8 Distribution of the number of years with given deviations of JJAS mean precipitation from the climatological mean JJAS Indian Summer monsoon rainfall over Indian land (8–28 N and 70–90 E)

having deviation more than $+1$ as the excess years. Figure 8 shows the distribution of years with respect to their deviation from JJAS mean climatology precipitation over Indian land for IMD observations, and the two model simulations (AL3 and AL1). Out of the 28 years which were simulated, 19 fall in the range of -1 to $+1$ deviation (normal monsoon rainfall). There are six drought and three excesses years in IMD. AL3 simulates four droughts and five excesses and AL1 simulates three droughts and six excesses. Hence, in general, the model under estimates the number of droughts and over estimates the number of excesses. The year of extreme excess in IMD (deviation in the range 2–3) is 1988 and AL1 simulates this excess quite realistically, producing deviation of $+1.96$. The deviation produced by control run is $+1.18$.

6.7 Niño 3.4 SST anomaly and tropical rainfall

The SST anomaly over Niño 3.4 region has significant influence on the tropical precipitation (Webster and Yang 2006). In the present study, we look into the sensitivity of tropical precipitation to Niño 3.4 SST anomaly in AL1 and AL3 simulations. Figure 9 shows the correlation between Niño 3.4 SST anomaly and precipitation anomaly over the tropics averaged over June-September for 28 years of simulation. High correlation between the precipitation and Niño 3.4 SST can be observed over the Pacific (150–240E, 10S–10N). The high negative correlation can be observed over Indonesian region and over equatorial Pacific region north of Australia. This correlation is captured well in both the simulations. The ISMR is negatively correlated to Niño 3.4 SST anomaly. The model produces this negative correlation satisfactorily with both the values of α. The feature which is distinctly different in the two simulations is the correlation over the West Pacific (0–20N, 100–150E), BoB and EIO. The precipitation over these regions is highly correlated to Niño 3.4 SST in AL1 simulation as compared to AL3 simulation. Since rainfall over EIO can play a role in modulating ISMR (Gadgil et al. 2007) and since precipitation over EIO is highly correlated to Niño 3.4 SST in AL1 simulation and not that much in AL3 simulation, it is worthwhile to look into the relationship of precipitation produced by the model over EIO and ISMR.

6.8 ISMR and IOD relationship

Apart from El-Niño, ISMR is also affected by variability associated with EIO Oscillation and Indian Ocean Dipole (IOD) (Gadgil et al. 2007). The IOD refers to the difference in SST anomalies over west (50–70E, 10S–10N) and east (90–110E, 0–10S) EIO. IOD is an anomalous state of air–sea interaction over western and eastern EIO and it changes the atmospheric circulation over Indian Ocean and its surroundings. In IOD mode, the SST anomaly over west is opposite to that over east EIO. When the SST anomaly over WEIO (EEIO) is positive and that over EEIO (WEIO) is negative, there is an enhanced convection over WEIO (EEIO) and suppressed convection over EEIO (WEIO). This oscillation is called EQUINOO. EQUINOO modulates zonal wind over EIO, and hence affects southwest monsoon over India.

Gadgil et al. (2007) emphasized that EQUINOO played a major role in the drought in ISMR of 2002 and excess of 1994. Gadgil et al. (1998) showed that a majority of

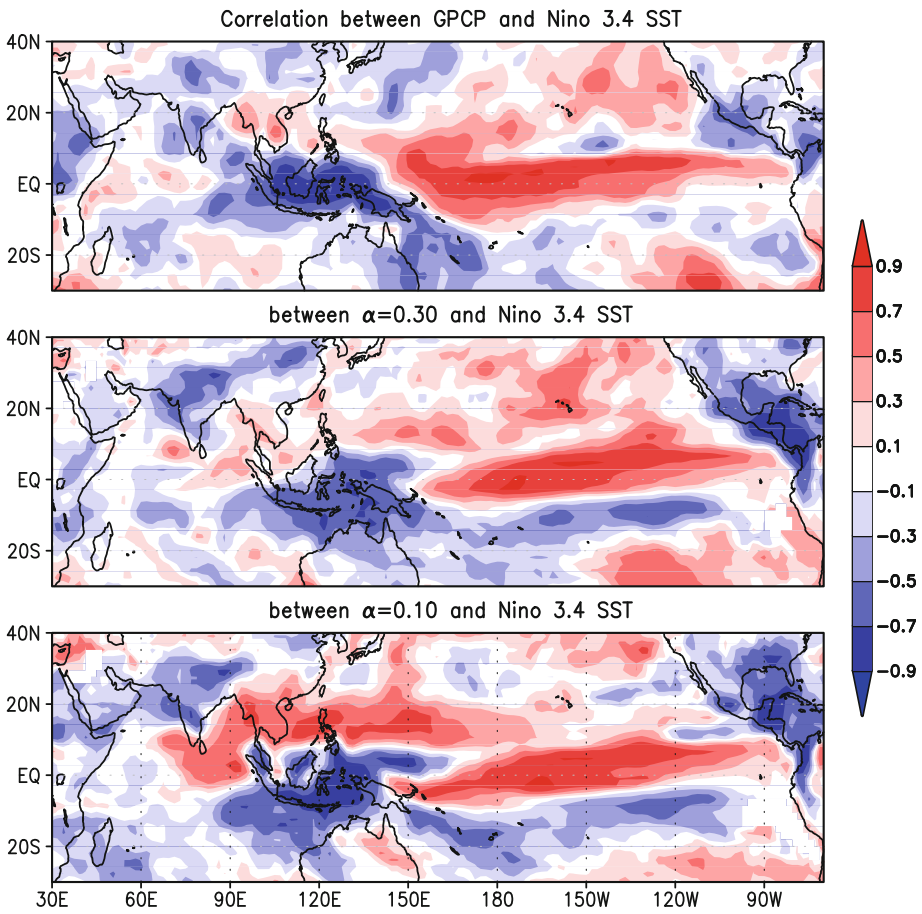

Fig. 9 Grid-by-grid correlation between interannual variation of June–September Niño 3.4 SST anomaly and precipitation anomaly in the observation (GPCP) and model (1982–2009)

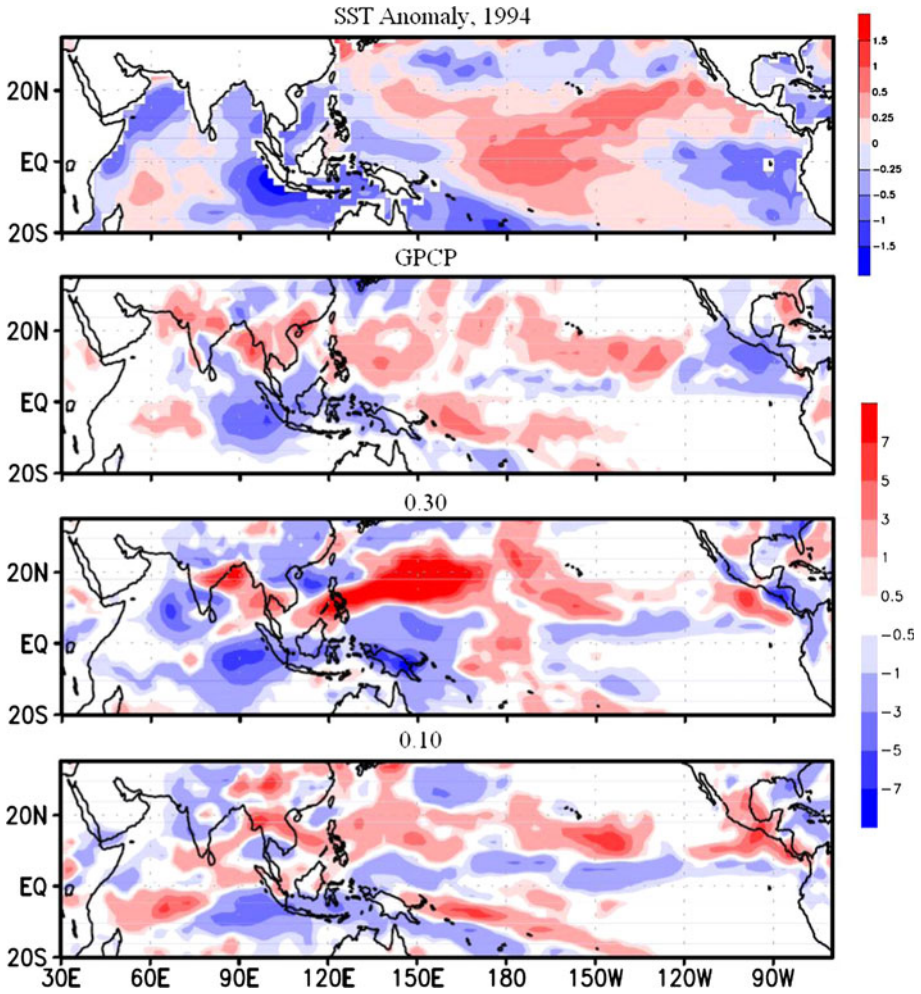

Fig. 10 JJAS mean SST and precipitation anomaly for 1994. SST is from Reynolds. Observed precipitation anomaly is from GPCP, and model with $\alpha = 0.30$ (control) and 0.10

models used in their study failed to capture the excess ISMR of 1994. We can say that the precipitation anomalies over west and east EIO can represent the atmospheric component of IOD provided there is coupling between SST anomaly and precipitation anomaly. Positive SST anomaly can result in positive precipitation anomaly due to enhanced evaporation and convection. Similarly negative SST anomaly can result in negative precipitation anomaly and we can use these anomalies to represent the atmospheric component of IOD based on precipitation. In Figs. 10 and 11, SST anomaly and corresponding precipitation anomalies over the tropics from GPCP and model is shown for 1994 and 2002. The 2 years shown in Figs. 10 and 11 are somewhat contrasting in the sense that 1994 was a strong and positive IOD event while 2002 was a weak and negative one. AL1 simulation is able to capture the observed (GPCP) IOD event over EIO. This feature is missing in the control simulation. However in 2002, simulations with both the values of α gives east–west precipitation anomaly indicating IOD in the model. This is not a very distinct feature in GPCP. The precipitation anomalies produced over West Pacific is also contrasting in the 2 years.

The interannual variability of IOD index based on SST anomaly and its effect on the precipitation over EIO is shown in Fig. 12. The IOD index is calculated as the difference in anomalies in precipitation over west (50–70E, 10S–10N) and east (90–110E, 0–10S) EIO. The precipitation index is the difference in anomalies over the same west and east EIO regions. In Fig. 12, we have normalized all the quantities using their standard deviation of 28 years. A positive value of IOD index is associated with positive SST anomaly over the west, and hence should result in more precipitation. The observed GPCP precipitation is well correlated to IOD index with a correlation coefficient of 0.89. This correlation coefficient is 0.68 in the AL3 simulation as compared to 0.64 in the AL1. Considering the fact that precipitation anomalies over EIO are well correlated to SST anomalies in both GPCP and simulations, one can use precipitation anomalies to represent atmospheric component of IOD. We should note here that SST was an input to the model and hence was same for both the

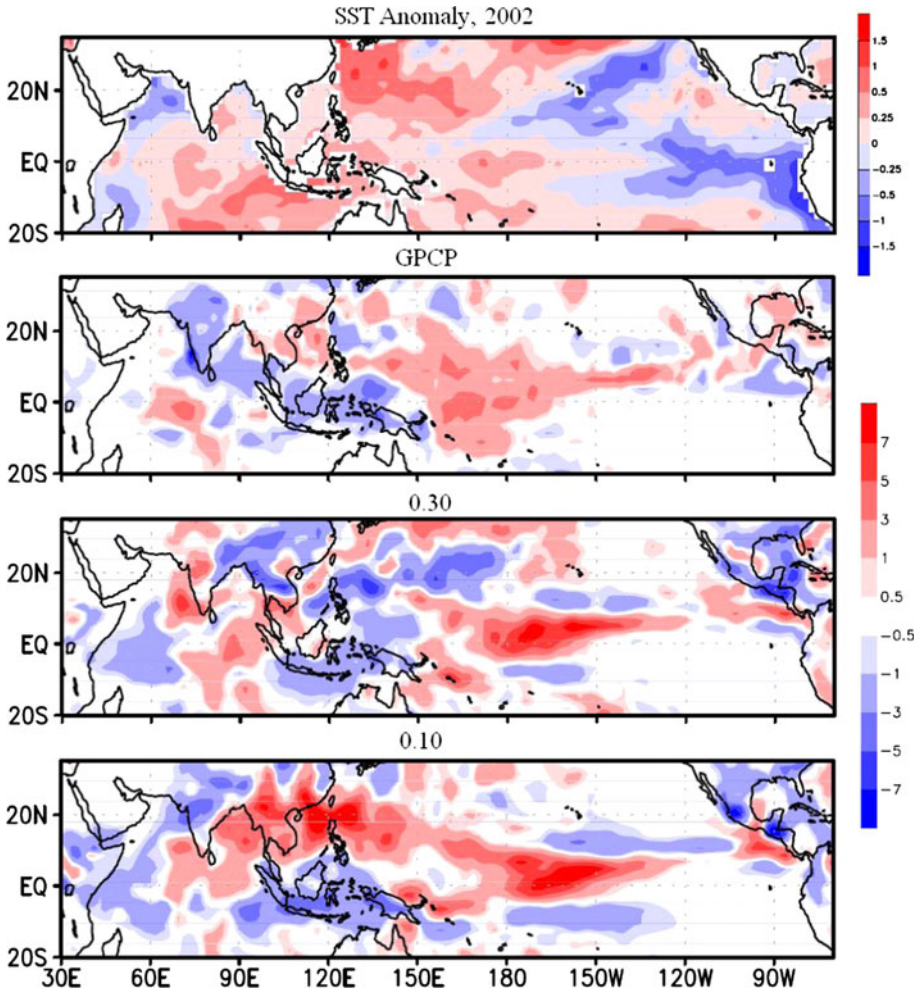

Fig. 11 Same as Fig. 10 but for 2002

AL3 and AL1 simulations. The change in correlation from 0.68 to 0.64 represents a change in ocean atmosphere coupling due to change in CATS.

Nanjundiah et al. (2013) have shown that convection over west equatorial Indian ocean (WEIO) (as measured using OLR) is significantly correlated with strength of the Indian monsoon. GPCP rainfall shows positive correlation in Fig. 13. We however find that WEIO is positively correlated in the AL3 and negatively in the AL1 simulation with ISMR. AL3 is in agreement with Nanjundiah et al. (2013). While the correlation coefficient over east EIO almost unaffected in the AL1 and AL3. The changing correlations over WEIO in the model shows that Indian Ocean–Indian Monsoon relationship is sensitive to prescription of CATS but it also clearly shows that improving this relationship needs more systematic study of ocean-atmosphere coupling over this region.

The links between ISMR, El Niño Southern Oscillation (ENSO) index and EQUINOO index were studied by Gadgil et al. (2007). They proposed that a positive value of ENSO and EQUINOO index favors positive ISMR anomaly and vise-versa. They came to the conclusion that a very high value of ENSO index (negative of Niño 3.4 SST anomaly) produces excessive ISMR irrespective of the value of EQUINOO index. Also, a very high value of EQUINOO index resulted into positive ISMR anomaly irrespective of the value of ENSO index. Similarly, a drought over Indian landmass was associated with highly negative values of either of the two indices. To study the similar relationships in the model, we have plotted Niño 3.4 SST anomaly, IOD index, and excess and droughts in ISMR in Fig. 14. In IMD observations, we can see that a very high value of IOD index can result into excessive ISMR even when we have weak positive Niño 3.4 SST anomaly. Similarly, if we have strong negative Niño 3.4 SST anomaly, we get excess ISMR even if IOD index is negative and unfavorable to ISMR. We can actually draw a line separating regions on the plot where we get excesses and droughts. In the control simulation (AL3), we can see that all the drought years lie in the region where IOD index is positive, while all the excess years lie in the region where Niño 3.4 SST anomaly is is negative. The correlation between Niño 3.4 SST anomaly, IOD index, and ISMR is not as clear as in IMD observations and we can not draw

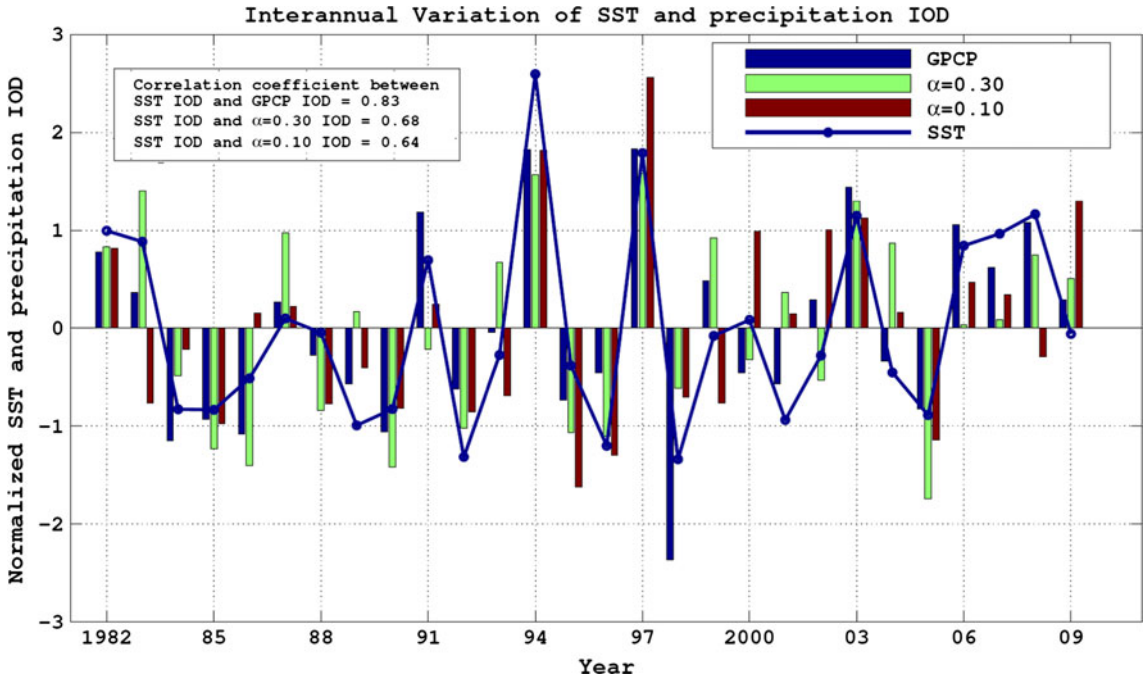

Fig. 12 Interannual variability of normalized (with SD) IOD index, normalized difference in GPCP precipitation, and the model precipitation anomaly over the same region where IOD index is calculated (see text for details)

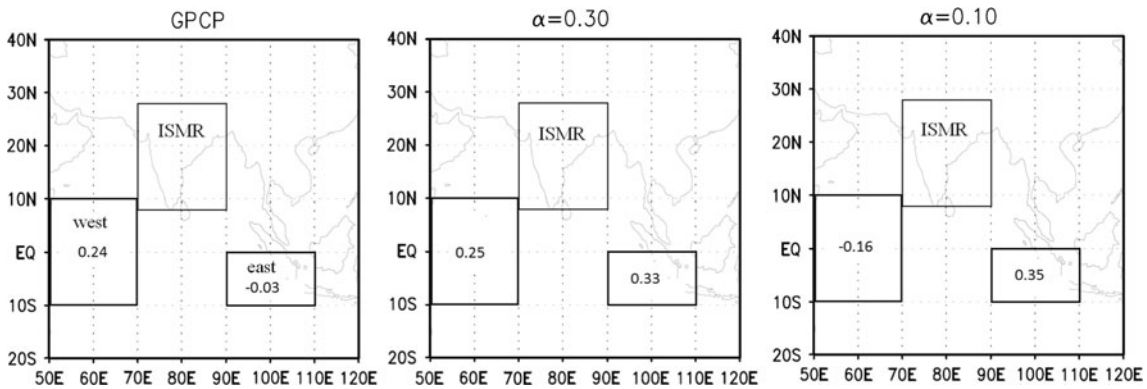

Fig. 13 Correlation coefficient (mentioned in the respective *box*) between JJAS mean east precipitation anomaly (the *right box*) and west precipitation anomaly (the *left box*) with JJAS mean ISMR (*central box* over India) from GPCP, and model simulation with $\alpha = 0.30$ and $\alpha = 0.10$

a line separating region of excesses and droughts in the figure. In the AL1 simulation, the model produces all the drought years on the right of Niño 3.4 SST anomaly = 0, and all the excess years to the left of it. IOD index does not seem to play as important a role in separating excess years from droughts.

7 Discussion and conclusion

In the present study, we have shown the sensitivity of interannual and intraseasonal variability of Indian summer monsoon to the choice of CATS or relaxation parameter in the RAS cumulus parameterization. The default value of relaxation parameter, which is the ratio of model time step to CATS, was 0.30. The time step in the model was 30 min. Hence, the assumed CATS in the model was 100 min. We performed another model simulation for 28 years starting from 1982 with relaxation parameter = 0.10. This corresponds to a CATS of 300 min (Jain et al. 2012).

The simulated climatological mean June–September precipitation was found sensitive to the value of relaxation parameter. It was seen that the model over-estimated the precipitation substantially over BoB and Arabian sea when relaxation parameter was 0.30. This over-estimated

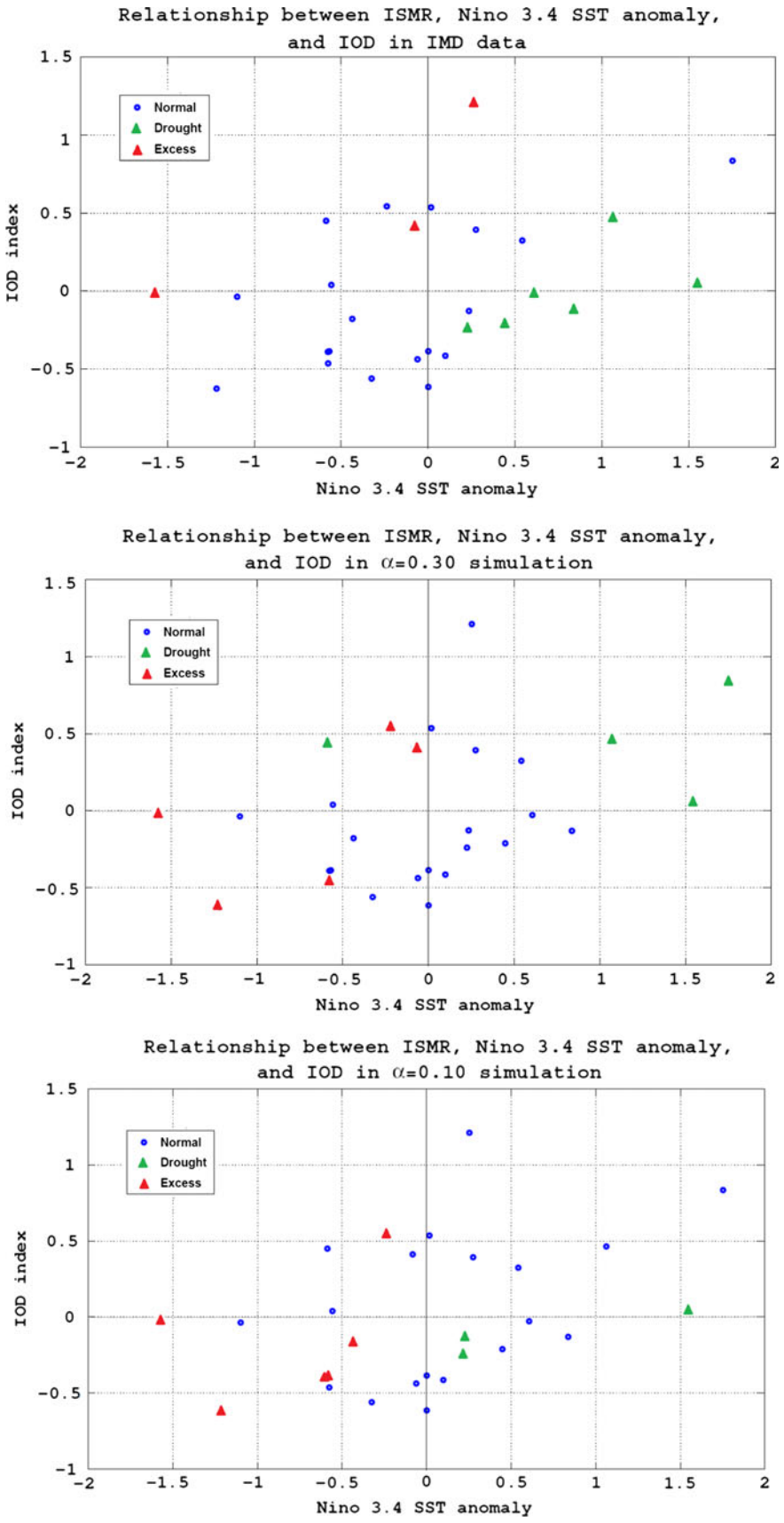

Fig. 14 Relationship between Indian summer monsoon rainfall anomaly, Niño 3.4 SST anomaly, and SST based IOD index

precipitation over the ocean reduced drastically with the smaller value of relaxation parameter (0.10). The RMSE over the Indian region (60–100E and 10S–40N) decreased when the relaxation parameter was reduced from 0.30 to 0.10. The reduced RMSE suggest that the climatological mean June–September precipitation over Indian region was simulated better when relaxation parameter was reduced to 0.10.

The monthly mean precipitation over the Indian land was also found sensitive to value of relaxation parameter. The model over-estimated monthly mean precipitation for all the months throughout the season irrespective of the value of relaxation parameter. The phase of monsoon precipitation (June–September) was found sensitive to relaxation parameter. The observed peak precipitation (IMD observations) during ISMR occurred in July. With the default value of relaxation parameter of 0.30, the model simulated peak precipitation in August. When relaxation parameter was reduced, the simulated peak precipitation was in phase with the observation i.e. in July. Improvements were also seen in JJAS daily mean precipitation. The time correlation between the simulation and observation was better in the AL1 compared to the control case (AL3). The time correlation was found to improve from 0.67 in the AL3 to 0.87 in the AL1.

The spectra for intraseasonal variability (10–90 days filtered data) of the daily precipitation over Indian land for first 23 years of simulation showed a 23 days dominant mode in the observation (IMD data). The slower CATS (rate of normalized CAPE consumption) with $\alpha = 0.10$ in the model favored a slower mode of 25 days time period, while faster CATS (AL3) in the model resulted into the faster mode (20 days) being dominant.

In the interannual variability of ISMR, the sign of simulated precipitation anomaly from 28 years climatology mean was found to be opposite in many of the years for the AL1 and the AL3 simulations. Especially during the strong El-Nino years, the simulated magnitude was very sensitive to relaxation parameter. During the strongest El-Nino years of 1982, 1987, and 1997, simulation in the control case produced much larger negative precipitation anomaly compared to that in the AL1 simulation. In four out of the seven El-Nino events, the sign of the anomaly was simulated correct when relaxation value was set to 0.10. The temporal correlation between Niño 3.4 SST anomaly and precipitation anomaly was -0.62 and -0.66 for AL1 and AL3 simulations respectively, indicating that the simulated ISMR is more sensitive to El-Nino in the control case compared to the case when relaxation parameter is reduced.

The spatial distribution of precipitation anomalies was also found to be sensitive to relaxation parameter. It can be seen that AL1 not just produces better seasonal mean precipitation as was seen in Jain et al. (2012), it also produces monthly mean precipitation and ENSO–ISMR relationship better. The interannual variability of precipitation anomalies over west and east EIO, which affects ISMR, was found to be sensitive to relaxation parameter. In the AL1 simulation, the correlation coefficient between precipitation based IOD index (normalized difference between west and east precipitation anomaly) and SST based IOD index decreased from 0.68 (with Al3) to 0.64 when relaxation time was increased. The correlation coefficient between GPCP precipitation based IOD and SST based IOD was 0.89. In the simulations correlation between ISMR and atmospheric component of west EIO was 0.25 for AL3, which is very close to that in GPCP, while in the AL1 it is -0.16, indicating that CATS plays a significant role in ocean-atmosphere coupling over the EIO.

To conclude, changing the adjustment time scale in the model (which is few hours) can significantly change not just the spatial distribution of the simulated precipitation, it can modify intraseasonal and interannual variability and coupling between Pacific Ocean, EIO and ISMR in a significant manner. Therefore the cloud adjustment timescales in mass-flux based schemes should be chosen in a careful manner for improved simulations of seasonal mean, intraseasonal and interannual variability of Indian summer monsoon in particular and tropical convection in general.

Acknowledgments RSN and AC are thankful to MoES/CTCZ and INCOIS for funding this research.

References

Alpert J, Kanamitsu M, Caplan P, Sela J, White G (1988) Mountain induced gravity wave drag parameterization in the NMC medium-range forecast model. In: Proceedings of 8th conference on numerical weather prediction, Baltimore, pp 726–733

Arakawa A, Schubert W (1974) Interaction of a cumulus cloud ensemble with the large-scale environment, Part I. J Atmos Sci 31:674–701

Bhanu Kumar O, Ramalingeswara Rao S, Ranganathan S, Raju S (2010) Role of intra-seasonal oscillations on monsoon floods and droughts over india. Asia-Pac J Atmos Sci 46:21–28

Chakraborty A (2010) The skill of ECMWF medium range forecasts during the year of tropical convection 2008. Mon Weather Rev 138:3787–3805

Chou M (1992) A solar radiation model for use in climate studies. J Atmos Sci 49:762–772

Chou M, Suarez M (1994) An efficient thermal infrared radiation parameterization for use in general circulation models. NASA Tech Memo 104606:85.

Das S, Mitra A, Iyengar G, Mohandas S (2001) Comprehensive test of different cumulus parameterization schemes for the simulation of the Indian summer monsoon. Meteorol Atmos Phys 78:227–244

Ding Y (2007) The variability of the Asian summer monsoon. J Meteorol Soc Jpn 85:21–54

Francis PA, Gadgil S (2013) A note on new indices for the equatorial Indian Ocean oscillation. J Earth Syst Sci 122(4):1005–1011

Gadgil S (2003) The Indian monsoon and its variability. Annu Rev Earth Planet Sci 31:429–467

Gadgil S, Rajeevan M, Francis P (2007) Monsoon variability: links to major oscillations over the equatorial Pacific and Indian oceans. Curr Sci 93:182–194

Gadgil S, Sajani S (1998) Monsoon precipitation in the AMIP runs. Clim Dyn 14:659–689

Goswami BN, Ajaya Mohan R (2001) Intraseasonal oscillations and interannual variability of the Indian summer monsoon. J Clim 14:1180–1198

Hahn D, Shukla J (1976) An apparent relationship between eurasian snow cover and Indian monsoon rainfall. J Atmos Sci 33:2461–2462

Hong S, Pan H (1996) Nonlocal boundary layer vertical diffusion in a medium-range forecast model. Mon Weather Rev 124:2322–2339

Ihara C, Kushnir Y, Cane M, De La Peña V (2007) Indian summer monsoon rainfall and its link with ENSO and Indian Ocean climate indices. Int J Climatol 27:179–187

Ihara C, Kushnir Y, Cane M, Kaplan A (2008) Timing of el nino-related warming and Indian summer monsoon rainfall. J Clim 21:2711–2719

Jain D, Chakraborty A, Nanjundiah RS (2012) On the role of cloud adjustment time scale in simulating precipitation with Relaxed Arakawa–Schubert convection scheme. Meteorol Atmos Phys 115:1–13

Kanamitsu M, Kumar A, Juang H, Schemm J, Wang W, Yang F, Hong S, Peng P, Chen W, Moorthi S et al (2002) NCEP dynamical seasonal forecast system 2000. Bull Am Meteorol Soc 83:1019–1037

Kang I, Jin K, Wang B, Lau K, Shukla J, Krishnamurthy V, Schubert S, Wailser D, Stern W, Kitoh A et al (2002) Intercomparison of the climatological variations of Asian summer monsoon precipitation simulated by 10 GCMs. Clim Dyn 19:383–395

Lee D, Tam C, Park C (2008) Effects of multicumulus convective ensemble on East Asian summer monsoon rainfall simulation. J Geophys Res 113:D24111

Mishra S (2011) Sensitivity of the Indian summer monsoon rainfall and its interannual variation to model time step. Atmos Res 101(1–2):67–77

Mishra S, Srinivasan J (2010) Sensitivity of the simulated precipitation to changes in convective relaxation time scale. Ann Geophys Copernic Group 28:1827–1846

Moorthi S, Suarez M (1992) Relaxed Arakawa–Schubert—a parameterization of moist convection for general circulation models. Mon Weather Rev 120:978–1002

Nanjundiah RS, Francis PA, Ved M, Gadgil S (2013) Predicting the extremes of Indian summer monsoon rainfall with coupled ocean-atmosphere models. Curr Sci 104(10):1380–1393

Pan HL, Mahrt L (1987) Interaction between soil hydrology and boundary-layer development. Bound-Layer Meteorol 38: 185–202

Pattanaik DR, Satyan V (2004) Sensitivity of Indian monsoon rainfall to different convective parameters in the Relaxed Arakawa–Schubert scheme. IITM research report No. RR-105

Rasmusson E, Carpenter T (1983) The relationship between eastern equatorial Pacific sea surface temperatures and rainfall over India and Sri lanka. Mon Weather Rev 111:517–528

Ratnam J, Sikka D, Banerjee S (2009) Simulation of 2006 monsoon using T170L42 AGCM: sensitivity to convective parameterization schemes. Int J Clim 29:289–303

Reynolds RW, Smith TM (1994) Improved global sea surface temperature analyses using optimum interpolation. J Climate 7:929–948

Shukla J, Mintz Y (1982) Influence of land-surface evapotranspiration on the earth's climate. Science 215:1498–1501

Slingo J (1987) The development and verification of a cloud prediction scheme for the ECMWF model. Q J Royal Meteorol Soc 113:899–927

Suppiah R (1996) Spatial and temporal variations in the relationships between the southern oscillation phenomenon and the rainfall of sri lanka. Int J Clim 16:1391–1407

Tebaldi C, Knutti R (2007) The use of the multi-model ensemble in probabilistic climate projections. Philos Trans R Soc A Math Phys Eng Sci 365:2053

Webster P, Yang S (2006) Monsoon and ENSO: selectively interactive systems. Q J R Meteorol Soc 118:877–926

Yoo JH, Kang I-S, Robertson AW (2010) Analysis of intraseasonal and interannual variability of the asian summer monsoon using a hidden markov model. J Clim 23:5498–5516

Zhang G, McFarlane N (1995) Sensitivity of climate simulations to the parameterization of cumulus convection in the Canadian climate centre general circulation model. Atmos Ocean 33:407–407

Zubair L (2002) El nino-southern oscillation influences on rice production in Sri lanka. Int J Clim 22:249–260